

APPLICATION OF MINIMUM ENTROPY DECONVOLUTION TO DETECT *pP* PHASE IN A SEISMOGRAM

RONG QIANG WEI

ABSTRACT. The hypocentral depth is a key requirement in seismology and earthquake engineering, but it is very difficult to be determined. The current accepted improvement is taking advantage of the depth phases, such as the *pP*, to constrain this parameter. However, it is not easy to pick such a phase in a seismogram from the other phases and the background noises. Here we propose the use of the minimum entropy deconvolution (MED) to detect it. Synthetic tests show that impulse(s) hidden in the seismic noises, eg. discrete unit impulses or the Gaussian mono impulses, can be detected completely. Further, we assume that the *pP* phase is an impulse-like signal buried in the Z component of the seismogram and applied this technique to 12 earthquakes in the International Association of Seismology and Physics (IASPEI) Ground Truth (GT) reference events list. Results show that 9 out of 12 earthquakes have absolute errors of less than 2.00 s for the travel-time differences of *pP*-P, and the maximum absolute error is 3.06 s. This demonstrates that the assumption above is reasonable, and this technique works well and effectively even for a single seismogram. Due to its little cost and effectiveness, this technique may be also useful in the starting points for other methods to detect *pP* phase.

Keywords:

earthquake, hypocentral depth, *pP* phase, MEC, Minimum entropy deconvolution (MED)

1. INTRODUCTION

The hypocentral depth is one of the four parameters for locating an earthquake. Its accurate determination is important for the study of many fields of the earth science, including continental dynamics, seismic hazard assessment, lithospheric rheology and structure, and plate tectonics. For example, Maggi et al. (2000) suggested that earthquakes in the continents are restricted in the upper brittle part of the crust and are either rare or absent in the underlying mantle. Based on this result, Jackson (2002) proposed a rheological model for the continental lithosphere in which the upper crust is strong but the mantle is weak. On the contrary, Chen and Yang (2004) argued that the mantle lithosphere is sufficiently strong with their observation that 11 earthquakes occurred in the mantle beneath the western Himalayan syntaxis, the western Kunlun Mountains, and southern Tibet. This controversy continues and new models have emerged based on the distribution of the hypocentral depths (eg., Burov, 2011; Chen et al., 2013; Prieto et al., 2017; Sunilkumar et al., 2019; Schulte-Pelkum et al., 2019).

There is agreement that hypocentral depth is the most difficult parameter to be determined in locating an earthquake, because of the trade-off with the origin time and as

it might be biased by lateral earth heterogeneities (Letort et al., 2014). A reliable way to estimate accurately it is through the detection of the depth phases (for example pP, sS, or sP) at teleseismic distances (eg., Abe, 1974; Engdahl et al., 1998; Bondár et al., 2004b; Craig, 2019). The reason is that the travel-time differences of pP-P and/or others (eg., sP-P, sS-S) are quite constant over large range of epicentral distances for a given depth (This can be found in the IASP91 tables (Kennett and Engdahl, 1991)). Therefore the hypocentral depth can be determined nearly independently of the epicenter distance, although there is indeed a little moveout of the depth phases with increasing epicentral distance (eg., Craig, 2019). For example, ISC-EHB have included 569,251 pP phases to constrain its hypocentral depths and the hypocentral depth uncertainties were significantly reduced (Engdahl et al., 2020).

Various methods have been developed to detect the pP phase, especially the travel-time differences of pP-P. These methods can be roughly classified into two categories depending on stacking or not. The common methods are (1) The cepstral method in frequency domain (Cohen, 1970; Bonner et al., 2002; Letort et al., 2014, 2015); (2) The time-domain equivalents of the 'cepstral' method (Kemerait and Sutton, 1982; Fang and van der Hilst, 2019); (3) The stacking method (Florez and Prieto, 2017; Craig, 2019). The cepstral method estimates the travel-time differences of pP-P through the peak 'cepstrum' in amplitude associated with separation times between various seismic phases from the Fourier transform of the (log) frequency spectrum of the waveform. The later two methods are those array-based and take advantage of the fact that the coherent arrivals (energy) can be enhanced while the incoherent noise (energy) can be suppressed by appropriate stacking of the signals across all array stations. With the increasing array networks, the methods based on array will be applied more and more widely. However, in many cases it is still necessary to develop new techniques to detect pP phase, especially for those seismograms observed only on a single-station.

Here we introduce such a technique of Minimum Entropy Deconvolution (MED). In the following sections, we will first introduce briefly the minimum entropy criterion (MEC) and MED, and validate the technique of MED with some synthetic tests. We then apply this technique to 12 earthquakes in IASPEI GT reference events list in which the arrivals of pP phases are picked with an high accuracy. Finally, we analyze the result and discuss another approach based on autocorrelation and MEC to detect echoes, and some related problems should to be noted.

2. MED AND ASSUMPTIONS

MED is a technique developed by Wiggins (1978) to extract the reflectivity information from seismic reflection recordings. In this technique, the seismic recording is assumed as a convolution model of a seismic wavelet with a series of reflectivity impulse response of the earth,

$$(1) \quad \mathbf{x}(\mathbf{t}) = \mathbf{w}(\mathbf{t}) * \mathbf{r}(\mathbf{t})$$

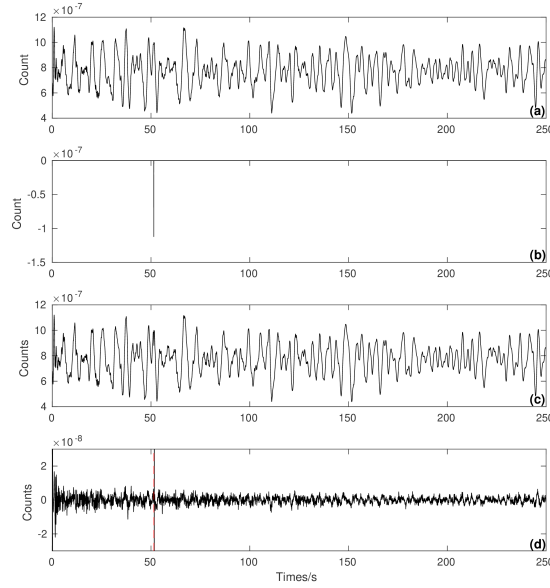


FIGURE 1. (a) is the seismogram for the Event 610471076 (Table 1) in IASPEI GT reference events list, which is recorded at the station DBIC. (b) shows a discrete unit impulse to be added. (c) is the synthetic waveform including the discrete unit impulse. (d) The series of reflectivity obtained by MED (Eq. (2)). The red dashed line marks the time at which the discrete unit impulse is added.

where $\{x(t); t = 1, N\}$ is the sample seismic recording (seismogram), $\{r(t); t = 1, N\}$ the reflectivity impulses, and $\{w(t); t = 1, M\}$ the seismic wavelet. $*$ denotes the convolution operator, ie., $x(t) = \sum_{t'=1}^M w(t')r(t-t')$.

Once the deconvolution filter $\bar{\mathbf{w}}(\mathbf{t})$ ($\bar{\mathbf{w}}(\mathbf{t}) \approx \mathbf{w}^{-1}(\mathbf{t})$) is computed, $\bar{\mathbf{r}}(\mathbf{t})$ (an estimate of $\mathbf{r}(\mathbf{t})$) is equal to $\bar{\mathbf{w}}(\mathbf{t}) * \mathbf{x}(\mathbf{t})$, that is,

$$(2) \quad \bar{r}(t) = \sum_{t'=1}^M \bar{w}(t')x(t-t')$$

Computing $\bar{\mathbf{w}}(\mathbf{t})$ is obviously a blind problem, because only $\mathbf{x}(\mathbf{t})$ is known in Eq. (1).

With the MED technique, $\bar{\mathbf{w}}(\mathbf{t})$ can be computed by maximizing the Kurtosis norm of the $\bar{\mathbf{r}}(\mathbf{t})$, ie.,

$$(3) \quad V_{\bar{r}} = \frac{\sum_{t=1}^N \bar{r}^4(t)}{\left[\sum_{t=1}^N \bar{r}^2(t)\right]^2}$$

And $\bar{\mathbf{w}}(\mathbf{t})$ can be obtained from the Eq. (4)

$$(4) \quad \mathbf{R}\bar{\mathbf{w}} = \mathbf{g}$$

where $R_{it'} = \sum_{t=1}^N x(t-i)x(t-t')$, and $g_i = \frac{[\sum_{t=1}^N \bar{r}^3(t)x(t-i)]}{V_{\bar{r}} \sum_{t=1}^N \bar{r}^2(t)}$, $i = 1, 2, \dots, M$.

Eq. (4) is highly nonlinear so that it can be solved iteratively. That is, assuming a value of $\bar{\mathbf{w}}$, computing \mathbf{R} and \mathbf{g} , solving Eq. (4) for \mathbf{g} , recomputing \mathbf{R} and \mathbf{g} , etc. Termination is defined as either a number of iterations, or a minimum change in Kurtosis norm between iterations. When $\bar{\mathbf{w}}(\mathbf{t})$ is obtained, $\bar{\mathbf{r}}(\mathbf{t})$ can be estimated from Eq. (2).

The advantage of this MED technique, as compared with other methods, is that it obviates the strong hypotheses over the phase characteristics of the seismic wavelet and the reflection series. The MED require only the simplicity of the output signal, in which the degree of simplicity is measured with the the Kurtosis norm of the output signal (Eq. (3)). Kurtosis norm has a feature that it is large for impulse-like signals. Wiggins (1978) has applied the MED to exploration seismic recordings and teleseismic core phases (the *PKP* and *PKKP*). Besides reconstructing the impulse-like signals, Wiggins (1978) found that the MED can reduce the low-frequency noise and is helpful to the phase shift and time separation between overlapping arrivals. Even more, some work demonstrated MED's effectiveness in the fault detection of rotating machine (Endo and Randall, 2007; McDonald and Zhao, 2017). We will further vindicate the effectiveness of the MED with some synthetic examples.

3. SYNTHETIC TESTS

Our synthetic background data is from a true seismogram for the Event 610471076 (Table 1) in IASPEI GT reference events list ¹(Bondár et al., 2004a, 2008; Bondár and McLaughlin, 2009). Here and after we only use BHZ component of the seismogram. This seismogram is recorded at the station DBIC. We cut it using between 0.25s and 250s after the P-wave arrival, which excludes the pP phase (0.18s after P arrival from the IASPEI GT bulletin) for this earthquake. Then we add one or two impulses into this seismograms and use MED to detect them. These impulses include the discrete unit impulse (Dirac) and the Gaussian mono-impulse. Here only the discrete unit impulse with a negative amplitude and the Gaussian mono-impulse with a negative starting amplitude are taken into account, because the pP phase is a solid-surface reflection.

Figure 1. (a) shows the seismogram we cut; And Figure 1. (b) gives a discrete unit impulse to be added, whose amplitude is $-0.1A_{\max}$ (A_{\max} is the maximum absolute amplitude of waveform in our time window). The synthetic data is shown in Figure 1. (c), ie., "(a)+(b)". The series of reflectivity (ie., $\bar{\mathbf{r}}(\mathbf{t})$) obtained by MED (Eq. (2)) are in Figure 1. (d), and we mark the true time at which the discrete unit impulse occurs with a red dashed line in this subfigure for comparison. It can be found that the this dashed line is coincident with the line occupying the smallest amplitude. That is to say, the discrete unit impulse

¹International Seismological Centre (2019), IASPEI Reference Event (GT) List, <https://doi.org/10.31905/32NSJF7V>

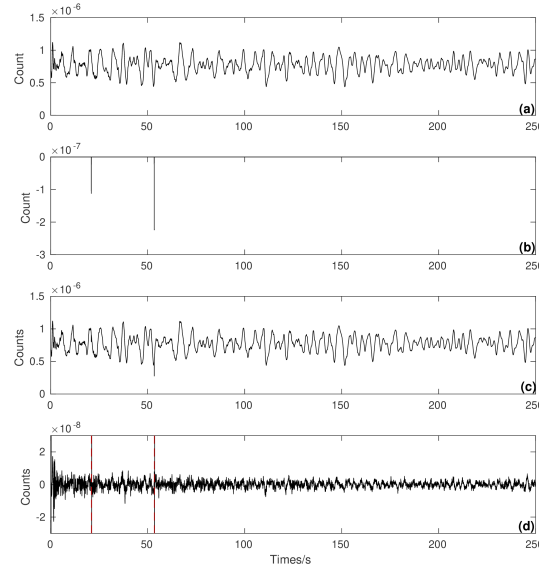


FIGURE 2. (a) is the seismogram for the Event 610471076 (Table 1) in IASPEI GT reference events list, which is recorded at the station DBIC. (b) shows two discrete unit impulses to be added. (c) is the synthetic waveform including the discrete unit impulses. (d) The series of reflectivity obtained by MED (Eq. (2)). The red dashed lines mark the true times at which the discrete unit impulses occur.

buried in the seismogram can be picked up; It is at the time at which the amplitude is the smallest (or the absolute value of the amplitude is the largest) in the series of reflectivity obtained by MED.

Figure 2 shows the result from burying two discrete unit impulses into the seismogram we used. These two discrete unit impulses have the amplitude of $-0.1A_{\max}$ and $-0.2A_{\max}$, respectively. The series of reflectivity are in Figure 2. (d), and we also mark the true times at which the discrete unit impulses occur with red dashed lines in this subfigure. It can be found that the these dashed lines are coincident with the lines occupying the smallest amplitudes. Further analysis shows that the second impulse with the larger amplitude is at the time at which the amplitude is the smallest, while the first impulse is located at the time at which the amplitude is the second smallest.

We have hidden more than two discrete unit impulses into the seismogram we cut, and all of them can be detected with the MED technique. They are also located at the times at which the amplitudes output from the MED are more smaller than those from the other phases or noises in the seismogram.

Figure 3 shows the result from burying a Gaussian mono-impulse into the seismogram we used. The impulse has a starting amplitude of $-0.4A_{\max}$. The series of reflectivity are in

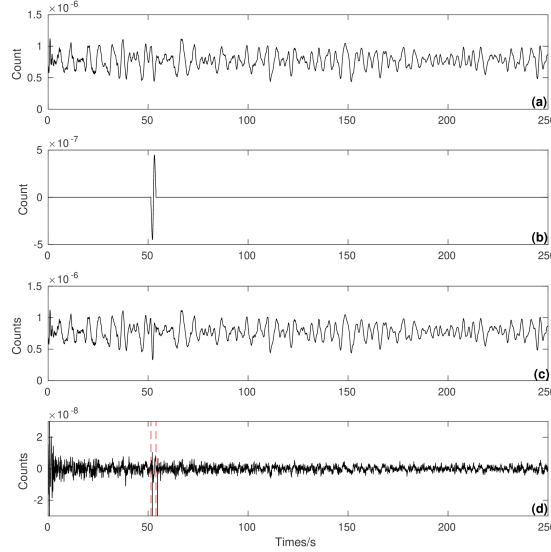


FIGURE 3. (a) is the seismogram for the Event 610471076 (Table 1) in IASPEI GT reference events list, which is recorded at the station DBIC. (b) is a Gaussian mono-impulse to be added. (c) is the synthetic waveform including the Gaussian mono-impulse. (d) The series of reflectivity obtained by MED (Eq. (2)). The red dashed lines mark the true times at which the impulse starts and ends.

Figure 3. (d), and we also mark the true times at which the Gaussian mono-impulse starts and ends with red dashed lines in this subfigure. It can be found that these dashed lines are almost coincident with the lines occupying the smallest amplitudes but with a little difference. Further analysis shows the time with the smallest amplitude is close to the end time of the Gaussian mono-impulse, while the time with the second smallest amplitude is close to the start time of this impulse. These above show that the Gaussian mono-impulse buried can be detected with MED but it has a little delay.

Figure 4 shows the result from hiding two Gaussian mono-impulses into the seismogram we used. The impulses have a starting amplitude of $-0.4A_{\max}$ and $-0.6A_{\max}$, respectively. The series of reflectivity are in Figure 4. (d), and we also mark the true times at which the Gaussian mono-impulses start and end with red dashed lines in this subfigure. It can be found the same properties as those when a single Gaussian mono-impulse is added. Further analysis shows the time with the smallest amplitude is close to the end time of the first Gaussian mono-impulse, while the time with the second smallest amplitude is close to the start time of this impulse; The time with the third smallest amplitude is close to the end time of the second Gaussian mono-impulse, while the time with the fifth smallest amplitude is close to the start time of this impulse; The time for the fourth smallest amplitude is

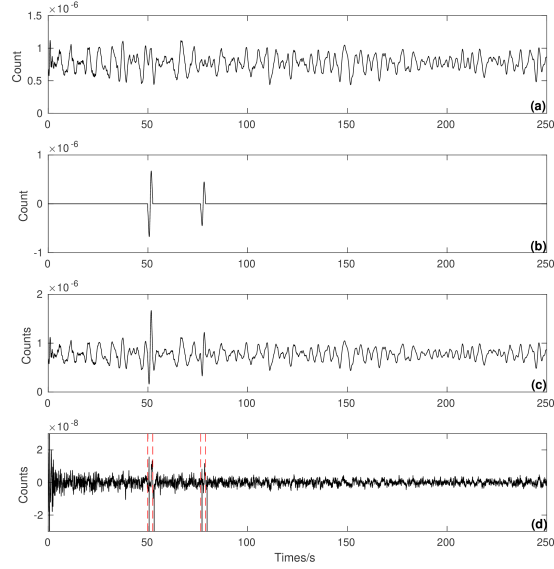


FIGURE 4. (a) is the seismogram for the Event 610471076 (Table 1) in IASPEI GT reference events list, which is recorded at the station DBIC. (b) shows two Gaussian mono-impulses to be added. (c) is the synthetic waveform including the Gaussian mono-impulses. (d) The series of reflectivity obtained by MED (Eq. (2)). The red dashed lines mark the true times at which two impulses start and end.

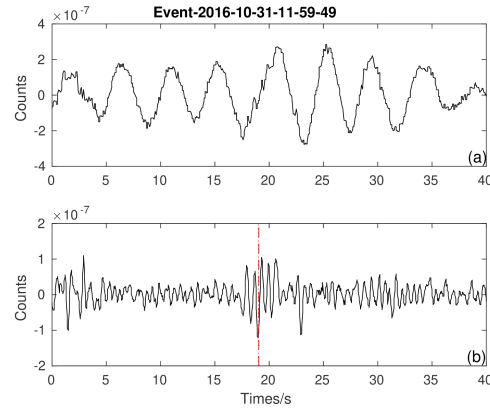


FIGURE 5. (a) is the seismogram for the Event 609632174 (Table 1) in IASPEI GT reference events list, only the part between 0.0s and 40s after P-wave arrival is shown. (b) The series of reflectivity obtained by MED (Eq. (2)). The red dashed line and dotted line mark the times occupying the first smallest and the second smallest amplitude, respectively.

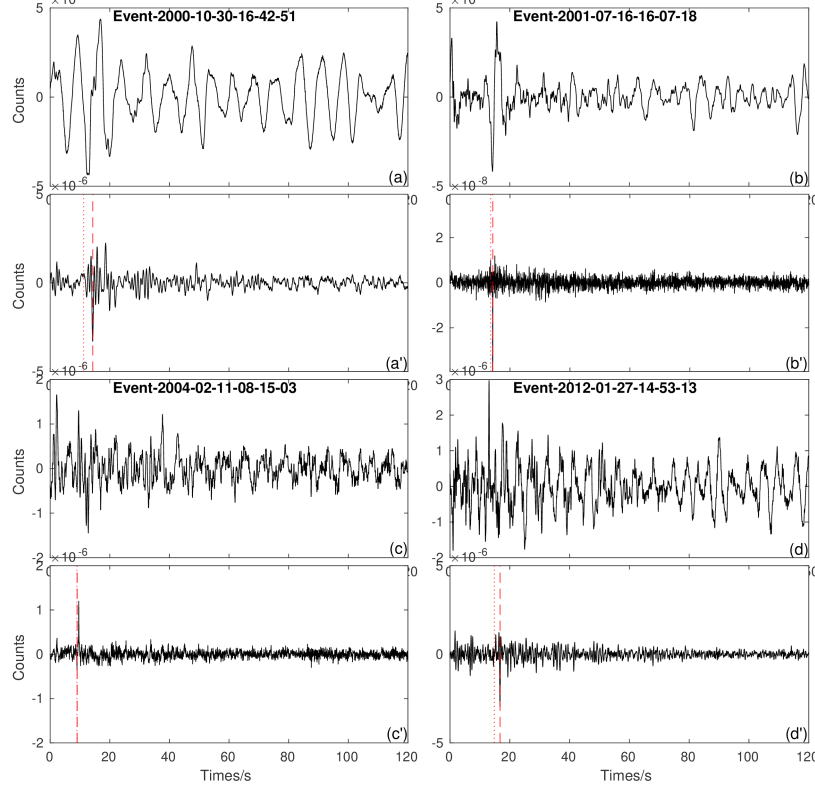


FIGURE 6. (a), (b), (c), (d) are the seismograms for the Event 1741194, 3160315, 7250126, and 604758676 (Table 1), respectively. (a'), (b'), (c'), and (d') are the corresponding series of reflectivity obtained by MED (Eq. (2)), respectively. The red dashed line in each subfigure of reflectivity series (eg., (a')) marks the time occupying the smallest amplitude; The red dotted line marks the time difference pP-P from the IASPEI GT bulletin.

close to the time origin of the time window. These above show that two Gaussian mono-impulses buried can be detected with MED but they have a little delay. Similar properties can be found for the cases when more than two Gaussian mono-impulses are added into the seismogram here.

4. APPLICATION TO 12 EVENTS IN IASPEI GT REFERENCE EVENTS LIST

pP phase is a near-source solid-surface reflection, but otherwise follow approximately the same path as the principal P phase through the rest of the earth. We assume that this reflective phase is an impulse-like signal in the P coda, and it corresponds to the smallest amplitude of the series of reflectivity obtained by MED. An example for verification of the feasibility of this assumption can be found from Figure 5. Figure 5 (a) is the seismogram for

TABLE 1. 12 earthquakes used from the IASPEI GT reference events list

| EVENTID ¹ | Date and Time | Latitude(°) | Longitude(°) | Station | t_{pP-P} (GT) ² | t_{pP-P} (MED) ³ |
|----------------------|---------------------|-------------|--------------|---------|------------------------------|-------------------------------|
| 1741194 | 2000/10/30/16:42:51 | 34.2920 | 136.2640 | MVU | 11.24s | 14.30s |
| 3160315 | 2001/07/16/16:07:18 | 32.8450 | 73.1300 | DPC | 13.6s | 14.3s |
| 7250126 | 2004/02/11/08:15:03 | 31.7106 | 35.4524 | STU | 8.99s | 9.05s |
| 604758676 | 2012/01/27/14:53:13 | 44.5433 | 10.0275 | OBN | 14.80s | 16.75s |
| 602754349 | 2013/03/31/07:02:37 | 42.6281 | 46.7839 | KHC | 10.90s | 10.65s |
| 602787145 | 2013/04/12/20:33:17 | 34.4134 | 134.8399 | GUMO | 1.34s | 3.35s |
| 605354327 | 2014/09/22/14:41:22 | -40.5433 | 175.9272 | FITZ | 8.5s | 9.0s |
| 608619656 | 2016/04/11/19:41:06 | -40.9108 | 175.5110 | CTAO | 5.83s | 8.18s |
| 611830427 | 2016/08/24/04:06:51 | 42.7612 | 13.1184 | BILL | 5.60s | 5.35s |
| 609439166 | 2016/09/11/13:10:08 | 42.0259 | 21.4598 | WMQ | 5.2s | 6.4s |
| 609632174 | 2016/10/31/11:59:50 | 45.8462 | 26.7773 | ARU | 17.40s | 19.05s |
| 610471076 | 2017/04/03/03:08:51 | -26.8715 | 26.7661 | DBIC | 0.18s | 0.05s |

¹ Unique id number specific to each IASPEI reference event.

² Data for columns 1-6 is from International Seismological Centre (2019), IASPEI Reference Event (GT) List, <https://doi.org/10.31905/32NSJF7V>.

³ Data is from this study.

the Event 609632174 (Table 1) in IASPEI GT reference events list (We cut the seismogram using between 0.0s and 120s but only show the part between 0.0s and 40s after P-wave arrival). Figure 5 (b) plots the series of reflectivity obtained by MED (The data processing before MED will be explained below). The red dashed line and dotted line mark the times with the first smallest and the second smallest amplitude, respectively. It can be found that: (1) These two lines are very close with a time difference of 0.05s; (2) The time occupying the smallest amplitude is 19.05s, which is close to that for pP phase (17.4s after P arrival from the IASPEI GT bulletin). Combining with the synthetic tests above, it is clear that pP phase can be described by a discrete unit impulses rather than a Gaussian mono-impulse (unless its duration is very very short), and it can be picked up through the smallest amplitude of the series of reflectivity obtained by MED.

Based on the experiences above, we apply the MED technique to 12 earthquake events in the IASPEI GT reference events list. Some information on these events is shown in Table 1. As mentioned earlier, only the component of "BHZ" is used here for all the events. For each seismogram, data processing includes: (1) Removing the spikes with a median filter; (2) Interpolating the missing values; (3) Detrending the seismogram to remove the linear drift; (4) Cutting the seismogram using between 0.0s and 120s after P-wave arrival according to the IASPEI GT bulletin; (5) Calculating the series of reflectivity obtained by MED; (6) Picking up the pP phases through the smallest amplitude of the reflectivity series in (5).

Results are shown in Table 1 and Figure 6-8. In each of the Figure 6-8, (a), (b), (c), (d) are the seismograms for the 4 Events (Table 1), respectively. (a'), (b'), (c'), and (d') plot the corresponding series of reflectivity obtained by MED (Eq. (2)), respectively. The red dashed line in each subfigure of reflectivity series marks the time occupying the smallest amplitude, namely the time difference $pP-P$; The red dotted line marks time difference $pP-P$ from the IASPEI GT bulletin. It can be seen from these figures that two lines (dashed

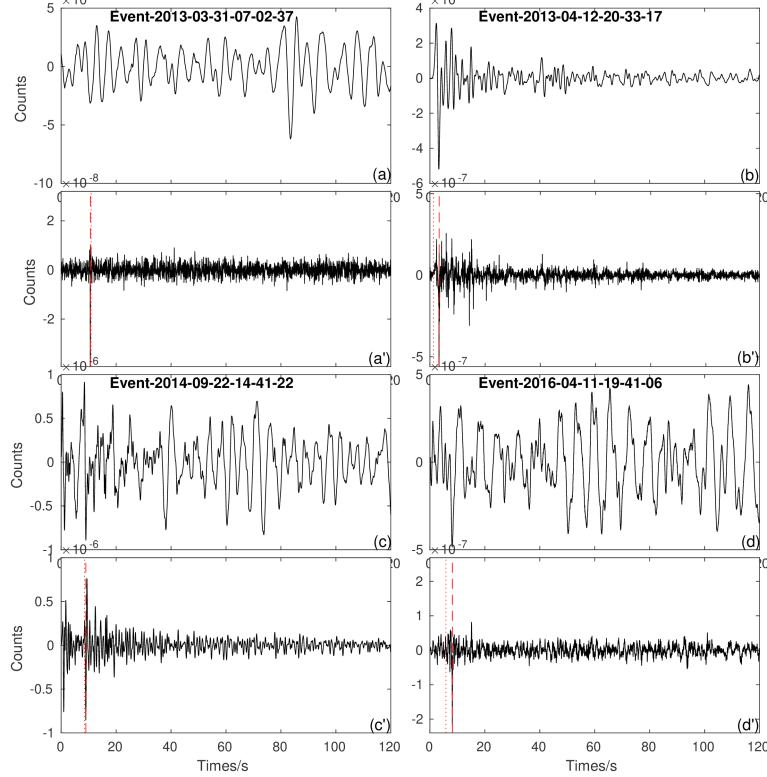


FIGURE 7. (a), (b), (c), (d) are the seismograms for the Event 602754349, 602787145, 605354327 and 608619656 (Table 1), respectively. (a'), (b'), (c'), and (d') are the corresponding series of reflectivity obtained by MED (Eq. (2)), respectively. The red dashed line in each subfigure of reflectivity series (eg., (a')) marks the time occupying the smallest amplitude; The red dotted line marks the time difference pP-P from the IASPEI GT bulletin.

and dotted line) in Figure 6 (b'), Figure 6 (c'), Figure 7 (a'), Figure 7 (c'), Figure 8 (a'), Figure 6 (d') are very close, while they are far apart in Figure 6 (a'). From Table 1 it can be found that the errors for event 3160315, 7250126, 602754349, 605354327, 611830427, and 610471076 are less than 1s, while error for event 1741194 is 3.06s. The smallest error is 0.06s for event 7250126, which also can be seen from Figure 6 (c'). These results show the technique of MED works well and effectively even for a single seismogram.

5. DISCUSSIONS

5.1. Limitations with the MED. The method of MED has many advantages, but it also has some limitations. The first limitation with the MED is how to determine the length (M) of the deconvolution filter $\bar{\mathbf{w}}(\mathbf{t})$. Our experiences show that too long or too short M

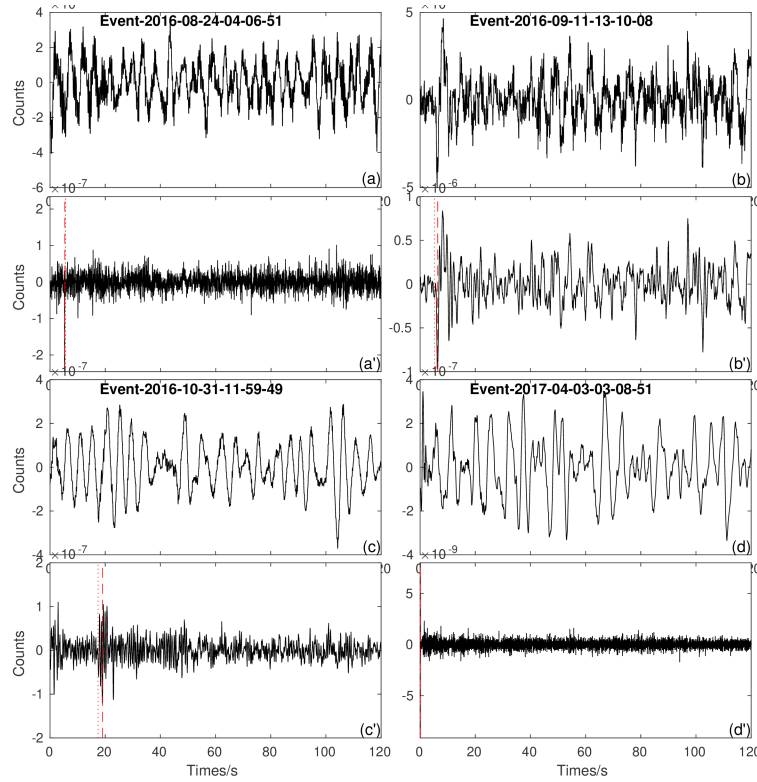


FIGURE 8. (a), (b), (c), (d) are the seismograms for the Event 611830427, 609439166, 609632174, and 610471076 (Table 1), respectively. (a'), (b'), (c'), and (d') are the corresponding series of reflectivity obtained by MED (Eq. (2)), respectively. The red dashed line in each subfigure of reflectivity series (e.g., (a')) marks the time occupying the smallest amplitude; The red dotted line marks the time difference pP - P from the IASPEI GT bulletin.

will lead to different but incorrect results, and the appropriate M depends on the input data. Unfortunately, such appropriate filter length M cannot be foreseen straightforwardly. A good way is trying filters of different lengths and examining the outputs to search this filter length. Obviously, this is an empirical approach. Here we select the filter length according to a minimum change in Kurtosis norm between filtering lengths, which is a good approximation but still not the perfect way. Besides, Eq. (4) is highly nonlinear so that it can be solved iteratively. The iterative solution may not lead to a unique maximum value for $V_{\bar{r}}$, and it needs a good initial solution. In our tests, there are failure examples which present incorrect arrival time of pP . Therefore sometimes this method will be used with the aid of other methods, to obtain a reliable solution.

Here we assume that only pP phase is included in the P coda, it corresponds to the smallest amplitude of the reflectivity series from the MED. This is the second limitation, because there may be other solid-surface reflected waves whose energy is stronger than pP phase, perhaps sP phase for example. At this time, our assumption are likely to obtain sP phase rather than pP phase. Besides, we have not considered the polarity of pP waves. If the polarity of pP phase is opposite to our assumption, it should be picked up from the positive amplitude in the reflection series from the MED. But these problems arise not only for MED, but also for other technique. In this sense, MED may be useful in obtaining an independent starting point for other schemes which require a reasonable arrival of pP phase.

The third limitation is that we assume that pP phase is an impulse-like signal in the P coda, while sometimes pP is more likely to be a wide harmonic. At this time, we may detect its end time instead of its start time with the MED technique. In this way, the time for pP phase obtained will be delayed.

5.2. Another technique to detect echo based on MEC. In many cases (for example in the cepstral method) a signal $x(t)$ is assumed as the sum of a direct wave $f(t)$ and one or two echoes which have the same frequency content as the $f(t)$ with only delays in time, as indicated in Eq. (5):

$$(5) \quad x(t) = f(t) + a_1 f(t - t_1) + a_2 f(t - t_2)$$

where $a_1, a_2 \in [-1, 1]$ are two amplitude coefficients; t_1, t_2 are time delays.

If $a_1(|a_1| > |a_2|)$ or $a_2(|a_1| < |a_2|)$, is known, $f(t - t_1)$ or $f(t - t_2)$ can be exactly determined with the technique of autocorrelation adding filtering (eg., Buck et al., 2002). However, in most cases, a_1 or a_2 are unknown. With the MEC, ie., by maximizing the Kurtosis norm of the signal filtered, we can exactly pick up the $f(t - t_1)$ or $f(t - t_2)$. An example is shown in Figure 9, in which the $x(t) = f(t) - 0.4f(t - 0.1) - 0.1f(t - 0.24)$ and the echo of $0.4f(t - 0.1)$ is to be picked up. Assuming that $a_1 = -0.4$ is not known in advance, we use the technique of autocorrelation adding filtering based on MEC to detect it. Figure 9 (e) demonstrate the echo of $0.4f(t - 0.1)$ is detected successfully, even we add some random noises to $x(t)$ (Figure 10 (f)). The delay time is picked up exactly and simultaneously.

The cases when there is only one echo, or there are three echoes are also tested with the technique of autocorrelation adding filtering based on MEC here. The echo interested (with larger absolute amplitude coefficient) is successfully detected, and the delay time is picked up exactly when there are no random noises simultaneously. When there are random noises to be added to $x(t)$, sometimes the echo interested is not detected, especially the amplitude of the noises is larger than that of $x(t)$. This is the same to the case when there are two echoes above.

Unfortunately, we have not applied successfully this technique of autocorrelation adding filtering based on MEC to an actual seismogram. One possible reason is that the actual

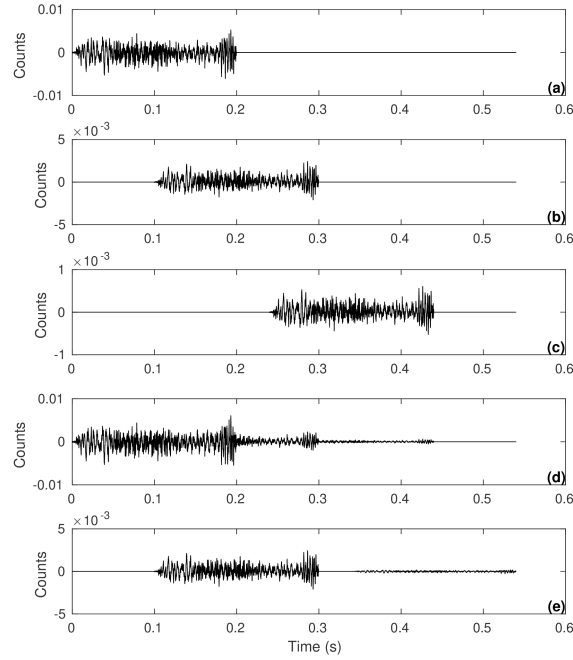


FIGURE 9. (a) The direct wave $f(t)$. (b) The first echo $-0.4f(t-0.1)$. (c) The second echo $-0.1f(t-0.24)$. (d) The signal $x(t) = f(t) - 0.4f(t-0.1) - 0.1f(t-0.24)$. (e) The echo $-0.4f(t-0.1)$ picked up with the technique of autocorrelation adding filtering based on MEC.

seismic waveforms we test do not meet the assumptions here. But this technique is worthy of further study.

5.3. t_{pP-P} varies with epicentral distance. As mentioned in the introduction, there is indeed a little moveout of the pP depth phases with increasing epicentral distance. That is, the travel-time differences of pP - P varies with epicentral distance. Craig (2019) demonstrate this with a synthetic example. Here we further illustrate this with the t_{pP-P} s from the IASPEI GT bulletin for two events (610471076 and 604758676, Table 1) in the IASPEI GT reference events list, as shown in Figure 11. It can be found that the moveout of the pP depth phases is clear, although there is scatter in the data. This should to be noted when we apply the usual stacking approaches to improve the detection of low-amplitude pP phases. Although the methods based on stacking may be more and more common in the future, this moveout of the pP demonstrate further that it is still necessary to develop new techniques to detect pP phase from the seismograms observed only on a single-station.

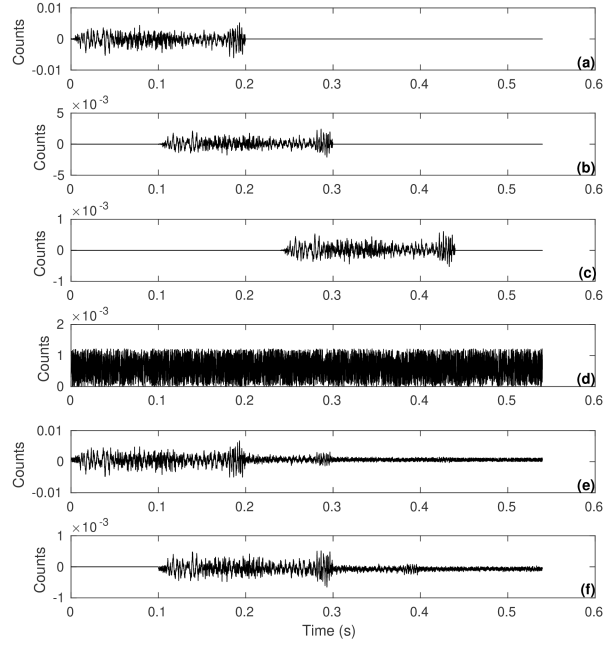


FIGURE 10. (a) The direct wave $f(t)$. (b) The first echo $-0.4f(t-0.1)$. (c) The second echo $-0.1f(t-0.24)$. (d) The random noises added to $x(t)$. (e) The signal $x(t) = f(t) - 0.4f(t-0.1) - 0.1f(t-0.24) + \text{noises}$. (f) The echo $-0.4f(t-0.1)$ picked up with the technique of autocorrelation adding filtering based on MEC.

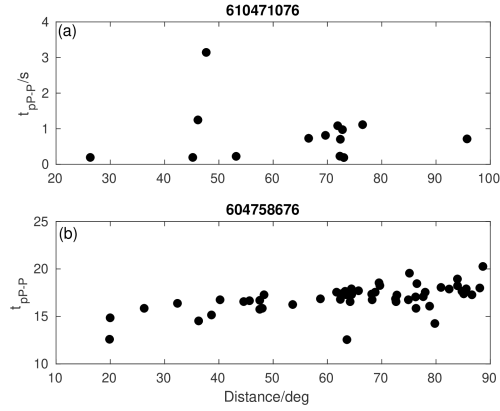


FIGURE 11. Variation of the t_{pP-P} with epicentral distance for two events in the IASPEI GT reference events list.

6. CONCLUSIONS

The technique of MED is effective to detect the *pP*-like phase when the seismic data meets the corresponding mathematical models and assumptions. Such effectiveness has been demonstrated from synthetic waveforms applications. MED is also effective to pick up *pP* phase from the actual seismogram, and the key to MED is how to determine the length of the deconvolution filter. It is a good way to select this filtering length according to a minimum change in Kurtosis norm between filtering lengths from our experiences.

REFERENCES

- [1] Abe, K., 1974. Fault parameters determined by near- and far-field data: The Wakasa Bay earthquake of March 26, 1963. *Bulletin of the Seismological Society of America*, 64, 1369–1382.
- [2] Bondár, I., Bergman, E. A., Engdahl, E. R., Kohl, B., Kung, Y., and McLaughlin, K. L., 2008. A hybrid multiple event location technique to obtain ground truth event locations, *Geophys. J. Int.*, 175, <https://doi.org/10.1111/j.1365-246X.2011.05011.x>
- [3] Bondár, I., Engdahl, E.R., Yang, X.P., Ghalib, H., Hofstetter, A., Kirichenko, V.V., Wagner, R.A., Gupta, I.N., Ekström, G., Bergman, E.A., Israelsson, H., and McLaughlin K.L., 2004a. Collection of a reference event set for regional and teleseismic location calibration, *Bull. Seismol. Soc. Am.*, 94, 1528–1545, <http://dx.doi.org/10.1785/012003128>.
- [4] Bondár, I. McLaughlin, K.L., 2009. A New Ground Truth Data Set For Seismic Studies, *Seismol. Res. Lett.*, 80, 465–472, <https://doi.org/10.1785/gssrl.80.3.465>.
- [5] Bondár, I., Myers, S.C., Engdahl, E. R., Bergman, E. A., 2004b. Epicentre accuracy based on seismic network criteria. *Geophysical Journal International*, 156, 483–496. doi:10.1111/j.1365-246X.2004.02070.
- [6] Bonner, J., Reiter, D., Shumway, R., 2002. Application of a cepstral F statistic for improved depth estimation, *Bull. Seismol. Soc. Am.* 92, 1675–1693.
- [7] Buck, J. R., Michael M.D., Andrew C.S., *Computer Explorations in Signals and Systems Using MATLAB*. 2nd Edition. Upper Saddle River, NJ: Prentice Hall, 2002.
- [8] Burov, E., B., 2011. Rheology and strength of the lithosphere, *Marine and Petroleum Geology*, 28, 1402–1443, doi:10.1016/j.marpetgeo.2011.05.008.
- [9] Chen, W.P., Yang, Z. H., 2004. Earthquakes beneath the Himalayas and Tibet: Evidence for strong lithospheric mantle. *Science*, 304(5679), 1949–1952.
- [10] Chen, W. P., Yu, C. Q., Tseng, T. L., Yang, Z., Wang, C. Y., Ning, J., Leonard, T., 2013. Moho, seismogenesis, and rheology of the lithosphere. *Tectonophysics*, 609, 491–503.
- [11] Cohen, T. J. ,1970. Source-depth determinations using spectral, pseudoautocorrelation and cepstral analysis, *Geophys. J. Roy. Astron. Soc.* 20, 223–231, doi: 10.1111/j.1365-246X.1970.tb06065.x.
- [12] Craig T. J. ,2019. Accurate depth determination for moderate-magnitude earthquakes using global teleseismic data. *Journal of Geophysical Research: Solid Earth*, 124. Doi: 10.1029/2018JB016902
- [13] Endo, H., Randall, R., 2007. Enhancement of autoregressive model based gear tooth fault detection technique by the use of minimum entropy deconvolution filter, *Mechanical Systems and Signal Processing*, 21(2), 906 – 919.
- [14] Engdahl, E. R., Di Giacomo, D., Sakarya, B., Gkarlaouni, C. G., Harris, J., Storchak, D. A. ,2020. ISC-EHB 1964–2016, an Improved Data Set for Studies of Earth Structure and Global Seismicity, *Earth and Space Science*, 7(1), e2019EA000897, doi: 10.1029/2019EA000897.

- [15] Engdahl, E., van der Hilst, R., Buland, R., 1998. Global teleseismic earthquake relocation with improved travel times and procedures for depth determination. *Bulletin of the Seismological Society of America*, 88, 722–743.
- [16] Fang, H., van der Hilst, R. D., 2019. Earthquake depth phase extraction with P-wave auto-correlation provides insight into mechanisms of intermediate-depth earthquakes. *Geophysical Research Letters*. 46 (24): 14440-14449, doi:10.1029/2019GL085062.
- [17] Florez, M. A., Prieto G. A., 2017. Precise relative earthquake depth determination using array processing techniques, *J. Geophys. Res. Solid Earth*, 122, 4559–4571, doi:10.1002/2017JB014132.
- [18] Jackson, J., 2002. Strength of the continental lithosphere: time to abandon the jelly sandwich? *GSA Today*, September, 4-10.
- [19] Kemerait, R., Sutton, A., 1982. A multidimensional approach to seismic event depth estimation, *Geoexploration*, 20(1-2), 113–130.
- [20] Kennett, B.L.N., Engdahl, E. R., 1991. Travel times for global earthquake location and phase identification. *Geophys. J. Int.* 105, 429–466.
- [21] Letort, J., Guilbert, J., Cotton, F., Bondár, I., Cano, Y., Vergoz, J., 2015. A new, improved and fully automatic method for teleseismic depth estimation of moderate earthquakes ($4.5 < M < 5.5$): application to the Guerrero subduction zone (Mexico), *Geophys. J. Int.* (2015) 201, 1834–1848, doi: 10.1093/gji/ggv093
- [22] Letort, J., Vergoz, J., Guilbert, J., Cotton, F., Sebe, O., Cano, Y., 2014. Moderate earthquake teleseismic depth estimations: new methods and use of the comprehensive nuclear-test-ban treaty organization network data, *Bull. seism. Soc. Am.*, 104(2), doi:10.1785/0120130126.
- [23] Maggi, A., Jackson, J. A., Priestley, K., Baker, C., 2000. A re-assessment of focal depth distributions in southern Iran, the Tien Shan and northern India: do earthquakes occur in the continental mantle? *Geophysical Journal International*, 143, 629–661, doi: 10.1046/j.1365-246X.2000.00254.x.
- [24] McDonald, G., L., Zhao, Q., 2017. Multipoint Optimal Minimum Entropy Deconvolution and Convolution Fix: Application to vibration fault detection, *Mechanical Systems and Signal Processing*, 82, 461-477. doi: 10.1016/j.ymssp.2016.05.036.
- [25] Prieto, G. A., Froment, B., Yu, C., Poli, P., Rachel Abercrombie, R., 2017. Earthquake rupture below the brittle-ductile transition in continental lithospheric mantle. *Science advances*, 3(3), e1602642.
- [26] Schulte-Pelkum, V., Monsalve, G., Sheehan, A.F., Shearer, P., Wu, F., Rajaure, S., 2019. Mantle earthquakes in the Himalayan collision zone: *Geology*, 47, 815–819, doi: 10.1130/G46378.1
- [27] Sunilkumar, T. C., Earnest, A., Silpa, K., Andrews, R., 2019. Rupture of the Indian Slab in the 2011 Mw 6.9 Sikkim Himalaya Earthquake and Its Tectonic Implications, *Journal of Geophysical Research: Solid Earth*, 124(3), 2623-2637. doi:10.1029/2018JB015931.
- [28] Wiggins, R. A., 1978. Minimum entropy deconvolution, *Geoexploration*, 16(1-2), 21-35

COLLEGE OF EARTH AND PLANETARY SCIENCES, UNIVERSITY OF CHINESE ACADEMY OF SCIENCES, BEIJING, PRC, 100049

Email address: wrq1973@ucas.edu.cn